OPTIMAL DESIGN OF A COMPOSITE SCARF REPAIR PATCH UNDER UNIAXIAL TENSION LOAD

T.D. Breitzman[#], E.V. Iarve[*], B.M. Cook[#], R.P. Lipton[^]
[#]US Air Force Research Laboratory, 2941 Hobson Way, WPAFB, OH 45433-7750, US
[*]University of Dayton Research Institute, 300 College Park, Dayton, OH 45469, US
[^]Dept. of Mathematics, Louisiana State University, Baton Rouge, LA 70803, US
timothy.breitzman@wpafb.af.mil, endel.iarve@wpafb.af.mil

SUMMARY

An optimal design algorithm was used to determine the repair fiber angles that minimize the stress in the adhesive of the repair joint. The strength was predicted by analysis using the Critical Failure Volume (CFV) approach for fiber failure. Excellent agreement was seen between predicted and tested strengths.

Keywords: Composite, Scarf Repair, Strength, Fiber Failure, Interfacial Strength

INTRODUCTION

The use of flush or nearly flush repairs for composite structures to maintain strict aerodynamic outer mold line requirements is a technology that is increasingly becoming essential to maintaining composite dominated aircraft structures. Unfortunately, there are only a limited number of studies on scarf repairs and patches. The published studies have described both experimental and numerical/analytical evaluation of the strains and failure loads of tension and compression loaded test articles and some of the shortcomings of current capabilities (for example [1,2]).

The experimental work described here was completed as part of the thesis work of Cook [3]. The thesis work included the measurement and prediction of free-edge strains in straight scarfed composite coupons [4] and the testing of 13.31 cm × 57.15 cm (5.25 in × 22.5 in) virgin, scarfed unpatched, and scarfed patched specimens. The results of the virgin and scarfed unpatched specimens will not be discussed here.

An analysis package that uses independent spline approximations of the displacement components *u*, *v*, and *w* for each ply of a laminate is used here to provide accurate three-dimensional solutions for stresses and displacements in composite scarf joints. The analysis maintains continuity of strains and stresses throughout a homogenous ply or adhesive while allowing strain discontinuity at ply interfaces in order to achieve interlaminar traction continuity, not achievable using conventional finite elements. Results from the analysis program have been shown to be in excellent agreement with Moiré interferometry ply level results for open hole composite laminate coupons [5,6] and for bonded doubler patches [7].

SPECIMEN FABRICATION AND TESTING

Panels measuring 30 cm × 61 cm (12 in × 24 in) with a $[+45/0/-45/90]_S$ stacking sequence were manufactures using IM6/3501-6 graphite/epoxy unidirectional prepreg. The panels were trimmed and cut in half to yield 13.31 cm × 57.15 cm (5.25 in × 22.5 in) test specimens. The apparatus uses a diamond bit with a pneumatic grinder that is rotated around a 2.54 cm (1.0 in) center hole and translated to provide a repeatable scarf cutout. A 1:20 scarf angle was maintained for the specimens. Additionally, the apparatus was used to cut out the scarf patches from laminates identical to those of the parent specimens.

The scarf patches were bonded to the parent specimens using Cytec Fiberite's FM-300M-05 adhesive. Additionally, a single over-ply extending on to the parent specimen was added to the top of the scarf patch to help in load transfer between the patch and parent specimen. The adhesive, as well as the over-ply, were cured using a 176ºC (350 ºF) cure cycle. The specimens were instrumented with uniaxial and rosette strain gages to monitor the far field surface strains, the strains on the patch over-ply, and strains adjacent to the patch on the parent specimen during tensile loading of the specimens. At various plan view locations on the specimen, back-to-back (front and back of the specimen) gages were mounted to measure localized bending strains caused by eccentricity of the specimen response. Glass reinforced epoxy tabs were bonded to the specimens with EPON 828 epoxy, a room temperature cure bonding system with EPI-CURE 3140 as the hardener. The tensile load was introduced into the specimens in the tab region through bolted fixtures.

Prior to testing, the loading fixtures were bolted to the two ends of the specimens. The torque on the 13 bolts on each tab was maximized to provide maximum load transfer from the fixtures to the specimen through shear transfer. This was done to prevent net section failure along the fixture bolt line. Four scarfed/patched panels were tensile loaded to failure. Each specimen was placed in the load frame and the strain gage leads were soldered onto the gages. The specimens were loaded in displacement control at a tension rate of 1.27 mm (0.05 in.) per minute.

NEAT ADHESIVE PROPERTIES

The Poisson's ratio and thermal expansion properties of FM 300M were determined by testing a neat adhesive plaque fabricated by stacking several layers of adhesive film, having an areal density of 244 grams per square meter. Figure .a shows the axial and transverse stress-strain curves for the neat adhesive FM 300M tensile test specimens. It can be seen that the response is nonlinear with an initial elastic modulus of 3.1GPa and the Poisson's ratio was determined to be ν=0.38 and appeared practically constant. The initial tensile modulus and Poisson's ratio are consistent with the initial shear modulus on Figure 1.b. The shear response was obtained from manufacturer supplied KGR-1 test curves. The nonlinear elastic constitutive equations for the adhesive material considered only variation of the Young's modulii and assumed constant Poisson's ratio in accordance with the experimental observations. The shear modulus G was expressed as

$$G = \min\left[\frac{E_1(J_1)}{2(1+\nu)}, G_2(J_2)\right] \quad (1)$$

where the elastic modulus E_1 is a monotonic function of strain calibrated using cubic spline interpolation from the tensile testing results (see Figure .a) and is expressed through the dilatational strain invariant J_1. Similarly, G_2 is the shear modulus calibrated based on the KGR-1 test results (Figure .b) and is expressed though the distortional strain invariant J_2, where

$$J_1 = \varepsilon_1 + \varepsilon_2 + \varepsilon_3$$

$$J_2 = \sqrt{\frac{1}{2}((\varepsilon_1 - \varepsilon_2)^2 - (\varepsilon_3 - \varepsilon_2)^2 - (\varepsilon_1 - \varepsilon_3)^2)}$$

and ε_i - are the principle values of the strain. The Eqn.(1) was also used to predict the failure of adhesive. Critical values of the strain invariants were established from Figure 3, where the curve termination correspond to failure, so that J_{1c}=0.0078 and J_{2c}=0.84. After the strain values result in invariants exceeding one of these values, the shear modulus was set to a small value of G=1000Pa.

OPTIMIZATION

The downhill simplex optimization algorithm was used to determine the fiber orientations for the repair layers that minimized the peak von Mises stress in the adhesive region. It is worth pointing out that the nonlinear strength prediction algorithm was not directly used for optimization. Instead, the adhesive stress state was calculated using initial elastic properties. After the optimal stacking sequence was obtained, a nonlinear analysis for this particular patch composition was performed as described above and the repair failure load reported. To reduce the von Mises stress in the adhesive domain, the optimization algorithm adjusted the fiber orientations in the repair plies. Within one repair layer, the fiber orientation was uniform, but the orientations of each layer in the repair could change independently of the other repair layers. The downhill simplex global optimization method [8] was used to minimize the L^p norm of the von Mises stress in the adhesive domain, where

$$L^p = \sqrt[p]{\frac{1}{V}\iiint_V (\sigma_M)^p \, dV}$$

Use of the L^p norm instead of simply the von Mises stress enabled the algorithm to concentrate on reducing actual volumes of large stresses instead of focusing on near-zero-volume points in the adhesive domain arising in the linear elastic analysis as a result of singularities near the ply interfaces and adhesive edge. The value of p was chosen $p=12$ based on prior work [9]. Elastic properties of the composite and neat adhesive used in optimization analysis are reported in Table 1.

Table 1: Elastic properties of IM-7/3501-6 and FM-300

	IM-7/3501-6	FM-300
E_{11}	175 GPa	3.12 GPa
E_{22}	9.79 GPa	
G_{13}	5.52 GPa	1.13 GPa
G_{23}	3.68 GPa	
v_{13}	0.33	0.38
v_{23}	0.449	
α_{11}	3.60×10^{-7}/°C	62.64×10^{-6}/°C
α_{22}	25.2×10^{-6}/°C	

RESULTS AND DISCUSSION

Flush Repair

The optimal stacking sequence for the flush repair was found to be [+50/+47/-31/+68/+106/-72/-36/36] (see Table 2). This stacking sequence is non symmetric and requires additional consideration in terms of possible manufacturing and load induced tension bending interaction. We evaluated thermal mismatch induced as well as load induced warpage of the repair region for the configurations: idealized ply-by-ply replacement, offset [+45/+45/0/-45/90/90/-45/0], and the optimized stacking sequence. Figure 2.a illustrates the out-of-plane displacements along the top of the specimen for the ply-by-ply, offset, and optimized repair lay-ups due to cure stress of -150C, while Figure 2.b depicts the displacements resulting from the combined thermal cure and mechanical load. The material properties are all linear elastic. Displacement boundary conditions were applied as follows on the lateral x=±285.75 surfaces: $u_x=u_y=u_z=0$ in the case of thermal loading and $u_x=\pm0.05$, $u_y=u_z=0$ in the case of thermal-mechanical loading. The points plotted are taken along the full length, on the centerline (with respect to width), and on the top of the model (see Figure 2).

As expected, the ply-by-ply repair produces the least out-of-plane displacement because of its perfect matching of ply stiffness from adherend to repair. For both the purely thermal load (Figure 2.a) and the thermal-mechanical load (Figure 2.b), the dramatically unsymmetric optimized repair produces out-of-plane displacement magnitude similar to that of the offset repair, although in the opposite direction. Thus, using unsymmetric repair stacking sequences appears to produce shape distortions in line with distortions expected with traditional repair techniques in field conditions.

The stress distribution in the adhesive in the case of the different repair patch configuration is displayed in Figure . The line plots of the von Mises stress in the

adhesive from the bottom of the model (z = 0) to the top of the eighth-ply of the model (z = 8) are displayed. The points were chosen along the midline of the adhesive layer between the adherend and repair patch on the y = 0 axis. The areas of high von Mises stress are the areas attaching the 0 degree plies of the adherend to the repair patch or attaching the adherend to the 0 degree plies of the repair patch. The optimal design results in the lowest stress concentration in the adhesive at least in the elastic regime. It is achieved by favoring a softer patch to avoid excessive stress transfer through the adhesive, especially near the 0 degree plies in the adherend.

Repair with over-ply

The introduction of an over-ply increased the complexity of the model geometry. The schematics of the repair geometry with an over-ply are shown in Figure . The adhesive layer was continued from the flush repair onto the top of the parent laminate, creating a contiguous adhesive layer bonding the patch and over-ply to the parent laminate. This basic model was termed OP1, see Figure 4.a. For repairs in the field, adhesive is used to bond the over-ply to the adherend, but no adhesive is present between the over-ply and the repair patch, which are co cured. Since the adhesive layer thickness is 0.0762mm – 0.127mm, inclusion of the adhesive between the over-ply and the adherend required a slightly thicker over-ply to fill the space (see Figure .a). In reality, the excess volume created by requiring strict lamination is taken up by slight thickness nonuniformity of the adhesive.

In addition to this model, a hypothetical model, shown in Figure 4.b, termed OP2, was considered. The difference between the two over-ply repair models was the way the over-ply was attached to the adherends. In the case of the OP2 no adhesive between the over-ply and adherend was modeled and displacement continuity between the two directly applied. The purpose of the OP2 model was to isolate the over-ply peel-off, which is apparently suppressed, and the failure of the adhesive between the patch and the adherends.

Both over-ply repair models (OP1 and OP2) used the flush repair model as a baseline model. The flush repair part of the model was not changed in either overply repair case, and the adhesive layer thickness was 0.127 mm.

Model OP2 was used first to evaluate the effect of the over-ply on stress relief in the adhesive as well as to understand the driving factors for the over-ply angle definition. The adherend was the same eight-ply [+45/0/-45/90]s quasi-isotropic laminate with a ply-by-ply repair. Two over-ply angles were considered: 45°, coinciding with the top ply angle and 0° coinciding with the loading direction. The von Mises stress in the adhesive is compared for the case of zero, one, two, four, and eight ply thickness over-plies. The resulting von Mises stress distributions normalized by the maximum von Mises stress occurring in the ply-by-ply replacement without the over-ply and are given in Figure . Both over-ply orientations reduced the stress in the adhesive near the top zero degree ply in the adherend (normalized z coordinate between 6 and 7). Thicker over-plies resulted in larger reduction of the stress. Regardless of the over-ply thickness, both over-ply fiber orientations failed to affect the high-stressed volume near the bottom zero degree ply (normalized z coordinate between 1 and 2).

We next observed the effect of the over-ply angle on the maximum von Mises stress occurring in the adhesive domain. The repair lay-ups compared are the ply-by-ply, offset, and optimal design (optimized with no over-ply). The over-ply was then added to the model. The maximum von Mises stress was computed for over-ply fiber

orientations between -90 and 90 degrees and was normalized by the von Mises failure stress of the adhesive. Plots of the results for the two over-ply models are given in Figure . Without adhesive (in model OP2, Figure .a), the preference is clearly toward a near-zero degree over-ply. Indeed, it provides the most load transfer through the over-ply and, respectively, the most stress relief in the adhesive around the repair. In the more realistic case, OP1 (Figure .b), when the adhesive is used to connect the over-ply to the adherend, large peel stresses occur near the outer edge of the adhesive when a near-zero degree over-ply is used. Hence, the preference is 54 or -54 degrees for the over-ply fiber orientation to minimize the stress in the adhesive.

The optimal patch stacking lamination was determined for both over-ply models, as well. The results of all optimizations are shown in Table 2. The flush repair (Optimized Flush Repair) patch optimization was described in the previous section. The other columns show the OP1 and OP2 over-ply repair optimization results. In both cases, the fiber orientation in the over-ply was treated as an optimization variable independent of the other repair layers. The column Optimized OP2 used the OP2 overply model, while the column Optimized OP1 used the OP1 overply model.

The differences seen between the optimization results using models OP1 and OP2 reflect the trend discussed above. In the idealized case of the attached over-ply (OP2), its optimal orientation is calculated at 5.26° and the repair patch contains several near zero degree layers. This phenomenon is due the fact that load is able to be directly transferred from the adherend to the over-ply without loading the adhesive. Thus, the over-ply carries large loads and wants to be near zero degree orientation. This tendency, however, is different than the trend exhibited in both the flush (no over-ply) repair and the repair using adhesive to connect the over-ply to the adherend (OP1). Both of these optimal designs avoid the use of zero degree plies in the repair plies (including the over-ply).

Table 2: Results of optimizations

Adherend	**Optimized Flush Repair**	**Optimized OP2**	**Optimized OP1**
N/A	N/A	5.26	-54.7
+45	36	11.75	43.81
0	-36	-45.28	-37.44
-45	-72	0.11	-121.78
90	106	91.27	67.23
90	68	-12.12	15.00
-45	-31	-25.16	-54.14
0	47	48.47	44.78
+45	50	50.42	57.46

At last, the strength of the laminates with optimized repair patch was calculated. A nonlinear algorithm (both material and geometrically nonlinear) was utilized along with adhesive constitutive equations (1) for strength prediction. [9] lists the predicted strengths of the repairs and the strengths previously discussed. Excellent agreement was seen between the prediction and physical test results for the ply-by-ply repair with the over-ply. Optimal design results are only predictions (no physical test data). The optimal design predicted strength for the repair without the over-ply is 33% larger than

the ply-by-ply strength. The optimal design configuration using model OP1 pushed the repair strength up to 90% of the virgin material strength. The idealized design using model OP2 predicted a repaired strength of 103% of the virgin laminate strength. This result is brought out for illustration purposes only and implies an ideal contact between the over-ply and adherend. The increased strength is predicted due to additional load transfer in the over-ply.

CONCLUSIONS

Mechanics of the composite repair under tensile loading with and without overlay plies were examined for nontraditional patch ply orientations. Three-dimensional nonlinear analysis was performed for repair failure prediction, which occurred as a result of the failure in adhesive. Only cohesive failure inside the adhesive was taken into account with tensile strength properties measured on bulk adhesive and KGR-1 shear response. The failure of the adherend was predicted by a statistical criterion applied to tensile fiber failure mode only. Good baseline comparison for open hole scarfed panels and panels repaired by using standard ply by ply replacement patch composition was achieved.

Von Mises stress distributions in the adhesive were examined as a function of thickness and orientation of the over-ply for standard repair patch composition. Similar to the flush repair case, the adhesive stress peaks at the junction of the 0° plies, which coincided with the loading direction. It was shown that the over-ply only reduced the stress concentration at the 0° ply joint nearest to itself. Increasing the over-ply thickness had only a small effect on the stress concentration at the juncture of the 0° plies on the opposite side of the plate.

Multidimensional optimization was performed to calculate the repair patch ply orientations which reduce the Von Mises stresses in the adhesive. These optimal stacking sequences achieved significant reduction of the stress levels and resulted in predicted up to 85% and 90% strength restoration for flush and single ply thickness over-ply repair. These results are intended to illustrate additional design variables available for efficient composite repair design, namely the composition of the repair patch.

References

1. Soutis, C. and F.Z. Hu. “A 3-D Failure Analysis of Scarf Patch Repaired CFRP Plates”, *American Institute of Aeronautics and Astronautics, Inc.*, Paper number AIAA-98-1943 pp.1971-1977 (1998).

2. Found, M.S. and Friend, M.J., “Evaluation of CFRP Panels with Scarf Repair Patches,” Composite Structures, Vol. 32, pp. 115-122, (1995).

3. Cook, B.M, Experimentation and Analysis of Composite Scarf Joint, M.S. Thesis, Air Force Institute of Technology, March 2005.

4. Cook, B., Schoeppner, G., Palazotto, A., “Thermal and Mechanical Strain Fields in Composite Scarf Joints,” Proceedings of the American Society of Composites Conference, Philadelphia, PA, September 7-9, 2005.

5. Mollenhauer, D. and Reifsnider, K., “Measurements of Interlaminar Deformation along the Cylindrical Surface of a Hole in Laminated Composite Materials by Moiré Interferometry,” Composites Science and Technology, **60**(12-13), 2375, 2000.

6. Mollenhauer, D., “Interlaminar Deformation at a Hole in Laminated Composites: A Detailed Experimental Investigation Using Moiré Interferometry,” Ph.D. Dissertation, Virginia Polytechnic Institute and State University, 1997.

7. Schoeppner, G.A., Mollenhauer, D.H., and Iarve, E.V., ”Prediction and Measurement of Residual Strains for a Composite Bonded Joint,” *Mechanics of Composite Materials*, Vol. 40, No. 2, 2004, pp 119-134.

8. Press,W., Flannary, B.P, Teukolsky and Vetterling, W.T. (1989), Numerical Recipes, Cambridge, pp 690.

9. Iarve, E.V., Mollenhauer, D., and Kim, R. (2005). Delamination Onset Prediction in Joints by Using Critical Weibull Failure Volume Method. *Proceedings* of ICCM-15, Durban, SA.

ACKNOWLEDGEMENTS

The analytical portion of the work was funded by Air Force Office of Scientific Research under contract FA9550-07-1-0028 to the University of Dayton Research Institute.

a) b)

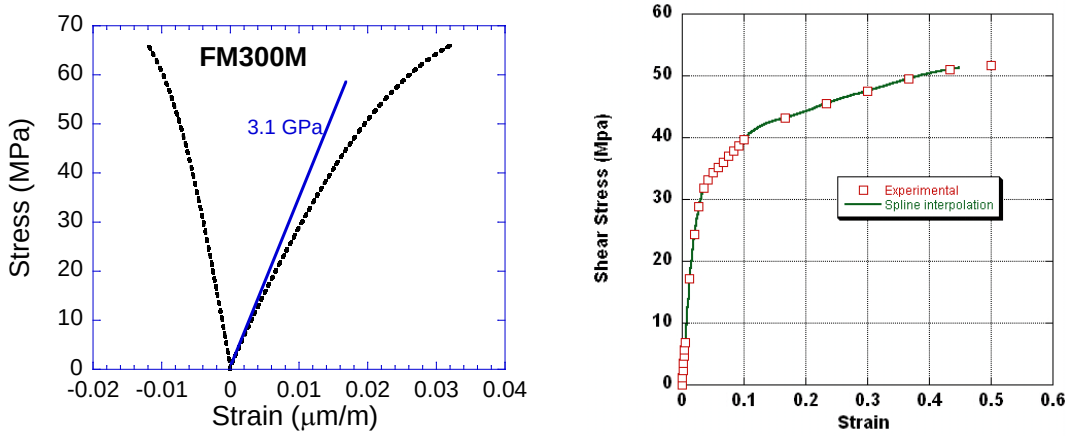

Figure 1: FM-300M tensile (a) and shear (b) response

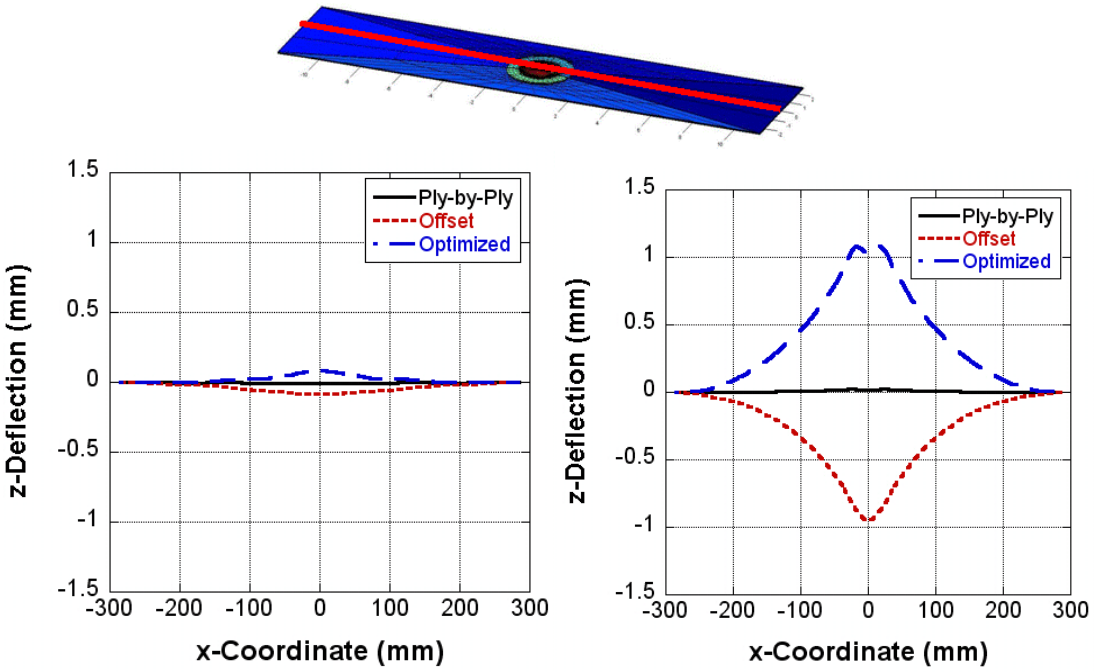

(a) (b)

Figure 2. Out-of-plane deflection for flush repairs for purely thermal (a) and thermo-mechanical (b) loads

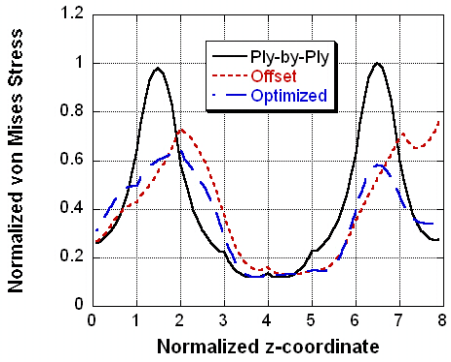

Figure 3: Normalized von Mises stress in the adhesive in the flush repair

(a) (b)

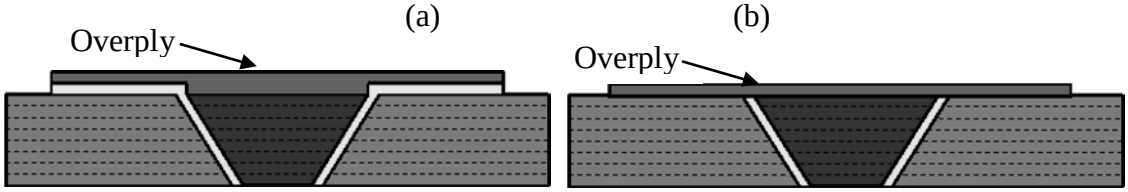

Figure 4: 2-D schematic of repair model geometries with an overply (OP1 and OP2)

(a) (b)

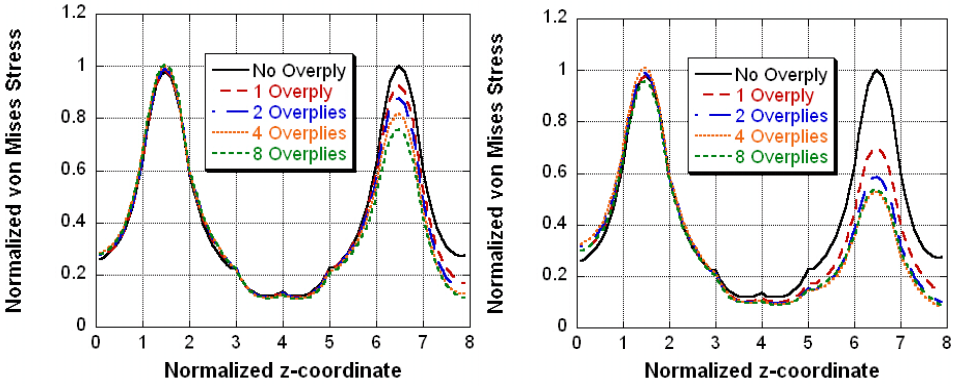

Figure 5: Effect of 45 degree overply (a) and 0 degree overply (b) thickness on the von Mises stress in the adhesive

(a) (b)

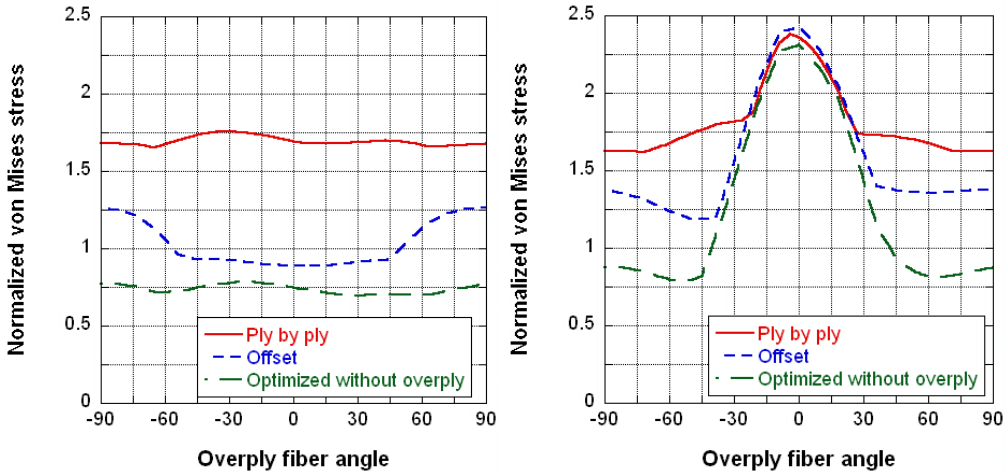

Figure 6: Effect of overply fiber orientation on adhesive in models OP2(a) and OP1(b)

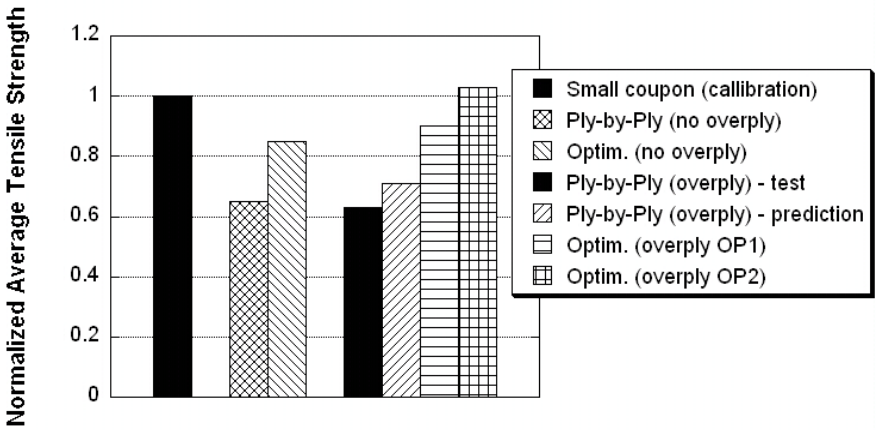

Figure 7: Predicted strength comparison for repaired laminates